

1 **Boron doped TiO<sub>2</sub> catalysts for photocatalytic ozonation of aqueous mixtures of**  
2 **common pesticides: Diuron, o-phenylphenol, MCPA and terbuthylazine**

3

4 **D.H. Quiñones<sup>1</sup>, A. Rey<sup>1\*</sup>, P.M. Álvarez<sup>1</sup>, F.J. Beltrán<sup>1</sup>, G. Li Puma<sup>2</sup>**

5 <sup>1</sup>*Dpto. Ingeniería Química y Química Física, Universidad de Extremadura, Avda. Elvas*  
6 *s/n 06006 Badajoz (Spain)*

7 <sup>2</sup>*Environmental Nanocatalysis and Photoreaction Engineering, Department of Chemical*  
8 *Engineering, Loughborough University, LE11 3TU, Loughborough (United Kingdom)*

9

10

11

12

13

14 **\*Corresponding author:**

15 Dr. Ana Rey

16 *Address: Dpto. Ingeniería Química y Química Física, Universidad de Extremadura, Avda. Elvas*  
17 *s/n 06006 Badajoz (Spain)*

18 *e-mail: anarey@unex.es*

19 *Phone: +34924289383*

20 *Fax: +34924289385*

21

22

23

24

25

26

27

28

29

30

31

32

1 **Boron doped TiO<sub>2</sub> catalysts for photocatalytic ozonation of aqueous mixtures of**  
2 **common pesticides: Diuron, o-phenylphenol, MCPA and terbuthylazine**

3  
4 **D.H. Quiñones<sup>1</sup>, A. Rey<sup>1\*</sup>, Pedro M. Álvarez<sup>1</sup>, F.J. Beltrán<sup>1</sup>, G. Li Puma<sup>2</sup>**

5 <sup>1</sup>*Dpto. Ingeniería Química y Química Física, Universidad de Extremadura, Avda. Elvas*  
6 *s/n 06006 Badajoz (Spain)*

7 <sup>2</sup>*Environmental Nanocatalysis and Photoreaction Engineering, Department of Chemical*  
8 *Engineering, Loughborough University, LE11 3TU, Loughborough (United Kingdom)*

9  
10 **Abstract**

11 TiO<sub>2</sub> and B-doped TiO<sub>2</sub> catalysts were synthesized using a sol-gel procedure. The  
12 photocatalysts were characterized by ICP-EOS, N<sub>2</sub> adsorption-desorption, XRD, XPS,  
13 and DR-UV-Vis spectroscopy. Four recalcitrant pesticides (diuron, o-phenylphenol, 2-  
14 methyl-4-chlorophenoxyacetic acid (MCPA) and terbuthylazine) were subjected to  
15 degradation by ozonation, photolytic ozonation, photocatalysis and photocatalytic  
16 ozonation using the prepared catalysts under simulated solar irradiation in a laboratory  
17 scale system-. The B-doped TiO<sub>2</sub> catalysts, with 0.5-0.8 wt.% of interstitial boron, were  
18 more active than bare TiO<sub>2</sub> for the removal and mineralization of the target compounds.  
19 The combination of ozonation and photocatalysis led to faster mineralization rates than  
20 the treatment methods considered individually and allowed the complete removal of the  
21 pesticides below the regulatory standards. The B-doped catalyst was stable and  
22 maintained 75% mineralization after three consecutive runs.

23  
24 **Keywords**

25 Photocatalytic ozonation, boron doped TiO<sub>2</sub>, boron leaching, pesticides, solar light.  
26  
27  
28  
29  
30  
31  
32  
33

## 1 1. Introduction

2 Water pollution and scarcity is a global concern. Agriculture is the industrial activity that  
3 has the major impact on aquatic ecosystems, due to the large volumes of water  
4 consumed (70% of the world accessible freshwater [1]) and the high content of organic  
5 substances (pesticides and fertilizers) which are dispersed in aqueous environments by  
6 runoff or leaching. Many pollutants found in water ecosystems are recalcitrant to some  
7 degree to biological and physicochemical processes that are conventionally used in  
8 wastewater treatment plants. In the last decades, Advanced Oxidation Processes  
9 (AOPs) have being pointed out as effective alternatives to deal with this kind of  
10 contaminants. These technologies can generate non-selective, highly reactive and  
11 short-life oxidizing species, which in turn can completely degrade organic pollutants  
12 through oxidation reactions [2].

13 Photocatalysis is one of the most successfully and extensively studied AOP. It involves  
14 the excitation of a semiconductor through the absorption of photons having energy  
15 greater than its band gap. This excitation promotes an electron from the valence to the  
16 conduction band, which triggers a series of oxidation-reduction reactions involving the  
17 excited electron and the generated hole at the valence band [2]. Recently, solar-driven  
18 TiO<sub>2</sub> photocatalytic oxidation has attracted considerable attention in water treatment  
19 applications. It offers the possibility of using solar energy to activate the semiconductor.  
20 However, due to the TiO<sub>2</sub> wide band gap (3.2 eV) its photoactivity is limited to  
21 ultraviolet irradiation ( $\lambda < 380$  nm) and thus less than 5% of the solar spectrum can be  
22 exploited [3]. In general, doping TiO<sub>2</sub> appears to be an effective way to overcome this  
23 limitation, since the photoactivity of the doped semiconductor may be extended to the  
24 visible-light region [4,5]. Boron doping constitute a way to accomplish it, since O atoms  
25 in the TiO<sub>2</sub> lattice can be substituted by B atoms mixing the p orbital of B with O 2p  
26 orbitals, narrowing the band gap and thus shifting the optical response into the visible  
27 range [5]. On the other hand, boron can also be located in interstitial positions of the  
28 TiO<sub>2</sub> lattice leading to the partial reduction of Ti(IV) to Ti(III), which could act as an  
29 electron trap enhancing the photocatalytic activity of TiO<sub>2</sub> [5,6].

30 Another way to improve the performance of TiO<sub>2</sub> photocatalytic systems is its  
31 simultaneous application with other AOPs, such as ozonation. The combined application  
32 of ozone and TiO<sub>2</sub> photocatalysis, known as photocatalytic ozonation, leads to a  
33 synergistic effect due to enhanced production of reactive oxygen species (ROS) such  
34 as hydroxyl radicals in comparison with the application of either single ozonation or  
35 single TiO<sub>2</sub> photocatalysis [7,8].

36 In this study, the degradation of four herbicides and pesticides: diuron (DIU), o-  
37 phenylphenol (OPP), 2-methyl-4-chlorophenoxyacetic acid (MCPA) and terbuthylazine  
38 (TBA), commonly found in water ecosystems, has been studied. Their molecular  
39 structures can be found in **Table S1** of the supplementary material. The degradation  
40 methods used were photocatalysis, ozonation, photolytic ozonation, and photocatalytic  
41 ozonation. Different boron doped TiO<sub>2</sub> photocatalysts (B-TiO<sub>2</sub>) were synthesized and  
42 used in the photocatalytic treatments.

## 1 2. Experimental section

### 2 2.1. Catalysts preparation

3 The synthesis of TiO<sub>2</sub> and B-TiO<sub>2</sub> catalysts was carried out following a sol-gel  
4 procedure previously reported [9]. Initially, a precursor solution was prepared by  
5 diluting the required amount of boric acid (Fisher Scientific) in 10 mL anhydrous  
6 ethanol (Panreac, 99.5%), then adding 4.26 mL tert-butyl titanate (Sigma Aldrich,  
7 97%), adjusting the pH to 3-4 with glacial acetic acid (Merck) and stirring for 30 min.  
8 After that, 20 mL ethanol were added to the precursor solution and the stirring was kept  
9 for 2 more hours. Ammonia aqueous solution (Fisher Scientific, 35%) was then added  
10 dropwise to reach pH 9. Afterward 10 mL ethanol was added and stirring was kept for  
11 another 30 min. The suspension was centrifuged and washed with ethanol three times.  
12 The resulting solid was dried at 60°C overnight, manually grinded and finally calcined  
13 at 500°C for 30 min. Catalysts with 3, 6, 9 and 12 wt.% of B were prepared. The  
14 nomenclature and some parameters of the catalysts are shown in **Table 1**. A fraction of  
15 catalysts with 6 and 12 wt.% of B were washed with ultrapure water to analyze the  
16 effect of B leaching.

### 17 2.2. Characterization of the catalysts

18 The characterization of the catalysts was carried out by inductively coupled plasma  
19 optical spectroscopy, N<sub>2</sub> adsorption-desorption, X-ray diffraction (XRD), X-ray  
20 photoelectron spectroscopy (XPS), and DR-UV-Vis spectroscopy.

21 Total B content of the catalysts was analyzed by inductively coupled plasma with an  
22 ICP-OES Optima 3300DV (Perkin-Elmer) after acidic microwave digestion of the  
23 samples.

24 BET surface area and pore structure of catalysts were determined from their nitrogen  
25 adsorption-desorption isotherms obtained at -196°C using an Autosorb 1 apparatus  
26 (Quantachrome). Prior to analysis the samples were outgassed at 250°C for 12 h under  
27 high vacuum (<10<sup>-4</sup> Pa).

28 The crystalline structure was analyzed by X-ray diffraction (XRD) using a Bruker D8  
29 Advance XRD diffractometer with a CuK $\alpha$  radiation ( $\lambda$  = 0.1541 nm). The data were  
30 collected from  $2\theta$  = 20° to 80° at a scan rate of 0.02 s<sup>-1</sup> and 1 s per point.

31 XPS spectra were obtained with a K $\alpha$  Thermo Scientific apparatus with an Al K $\alpha$   
32 (h $\nu$ =1486.68 eV) X-ray source using a voltage of 12 kV under vacuum (2x10<sup>-7</sup> mbar).  
33 Binding energies were calibrated relative to the C1s peak at 284.6 eV.

34 Diffuse reflectance UV-Vis spectroscopy (DR-UV-Vis) measurements, useful for the  
35 determination of the semiconductor band gap, were performed with an UV-Vis-NIR  
36 Cary 5000 spectrophotometer (Varian-Agilent Technologies) equipped with an  
37 integrating sphere device.

1 Transmitted photon flux through a catalyst suspension was analyzed by actinometrical  
2 measurements following the method proposed by Loddo et al. in [10], using the solar  
3 simulator described below with 250 mL of actinometrical solution and 250 mL of  
4 catalyst suspension at 0.33 g L<sup>-1</sup>. Incident radiation flux was determined with ultrapure  
5 water replacing the catalyst suspension and was found to be 8.96x10<sup>-4</sup> einstein min<sup>-1</sup>.

### 6 **2.3. Photocatalytic activity measurements**

7 Photocatalytic experiments were carried out in a laboratory-scale system consisting of  
8 a 250 mL pyrex made 3-neck round-bottom flask (8.8 cm outer diameter) provided with  
9 a gas inlet, a gas outlet and a liquid sampling port. The reactor was placed in the  
10 chamber of a commercial solar simulator (Suntest CPS, Atlas) equipped with a 1500 W  
11 air-cooled Xe lamp with emission restricted to wavelengths over 300 nm (quartz and  
12 glass cut-off filters). The emission spectrum of the solar simulator can be seen in  
13 **Fig.S1** of the supplementary material. The irradiation intensity was kept at 550 W m<sup>-2</sup>  
14 and the temperature of the system was maintained between 25 and 40°C throughout  
15 the experiments. If required, a laboratory ozone generator (Anseros Ozomat Com AD-  
16 02) was used to produce a gaseous ozone-oxygen stream that was fed to the reactor.

17 In a typical photocatalytic ozonation experiment, the reactor was first loaded with 250  
18 mL of an aqueous solution containing 5 mg L<sup>-1</sup> initial concentration of each pesticide (in  
19 a mixture). Then, the catalyst was added at a concentration of 0.33 g L<sup>-1</sup> and the  
20 suspension was stirred in the darkness for 30 min (dark adsorption stage). Then, the  
21 lamp was switched on and, simultaneously, a mixture of ozone-oxygen (5 mg L<sup>-1</sup> ozone  
22 concentration) was fed to the reactor at a flow rate of 10 L h<sup>-1</sup>. The irradiation time for  
23 each experiment was 2 h. Samples were withdrawn from the reactor at intervals and  
24 filtered through a 0.2 µm PET membrane to remove the photocatalyst particles.

25 Photolysis experiments (i.e. absence of catalyst and ozone), adsorption (i.e., absence  
26 of radiation and ozone), ozonation alone (i.e., absence of radiation and catalyst), and  
27 photolytic ozonation (i.e., absence of catalyst) were also carried out for comparative  
28 purposes.

29 Pesticides concentrations were analyzed by HPLC (Hewlett Packard) provided with a  
30 Kromasil C18 column (5 µm, 150 mm long, 4 mm diameter, Teknokroma). As mobile  
31 phase a mixture of acetonitrile (solvent A) and 0.1% (v/v) phosphoric acid solution  
32 (solvent B) was used at 1 mL·min<sup>-1</sup>. Initially the mobile phase composition was varied from  
33 40 to 25% solvent A in 12.5 min, then varied to 40% in 7.5 min and finally maintained at that  
34 composition for more 10 min. The retention times for DIU, MCPA, TBA and OPP were 10,  
35 15.2, 23.2 and 25.8 min, respectively. The detection system was set at 220 nm.

36 Total organic carbon content (TOC) was measured using a Shimadzu TOC-V<sub>SCH</sub> analyzer.  
37 Dissolved ozone was measured photometrically by following the indigo method at 600  
38 nm [11]. Ozone in the gas phase was continuously monitored by means of an Anseros  
39 Ozomat GM-6000Pro analyzer. Hydrogen peroxide concentration was determined  
40 photometrically by the cobalt/bicarbonate method at 260 nm [12]. Boron leached from  
41 the catalysts was determined photometrically after complexation with azomethine-H at

1 410 nm [13]. Photometric measurements were carried out in a UV-Visible  
2 spectrophotometer (Evolution 201, Thermospectronic).

3

### 4 **3. Results and discussion**

#### 5 **3.1. Catalysts characterization**

6 **Table 1** summarizes some characteristics of the B-doped TiO<sub>2</sub> catalysts. Firstly, it can  
7 be noticed that the amounts of B incorporated to the catalysts are much lower than the  
8 theoretical values. Similar results have been observed in previous studies where  
9 around only 5-10% of the theoretical B was introduced in the final catalyst following sol-  
10 gel synthesis techniques [14,15].

11 The structure of the catalysts was analyzed by means of XRD and diffraction patterns  
12 are shown in **Fig.1**. Anatase was identified as the only TiO<sub>2</sub> crystalline phase in all the  
13 catalysts together with the appearance of the sassolite boron structure (H<sub>3</sub>BO<sub>3</sub>) with the  
14 main diffraction peak at  $2\theta=28^\circ$  for the catalysts with B content equal or greater than  
15 the theoretical 6 wt.%. In addition, from the XRD patterns it can also be noticed that  
16 anatase diffraction peaks intensity decreased with the increasing B content. The  
17 crystallite size of anatase in the catalysts was calculated through Scherrer's equation.  
18 The values, which are shown in **Table 1**, reveal that the crystal size decreases with the  
19 increasing B content. This effect has been previously reported for similar catalysts and  
20 it has been attributed to the restrained TiO<sub>2</sub> crystal growing due to the existence of  
21 large amount of boron [16,17,18].

22 Textural parameters (BET surface area and total pore volume) were calculated from  
23 the adsorption-desorption isotherms presented in **Fig.S2** of the supplementary  
24 information and are summarized in **Table 1**. In general, the sol-gel synthesis procedure  
25 together with the relatively short time of calcination led to catalysts with fairly high  
26 surface areas. In addition, it can be observed that both, BET surface area and total  
27 pore volume, increased with the increasing B content, effect that can be attributed to  
28 the lower crystal size of the anatase phase in the B-TiO<sub>2</sub> catalysts [16].

29 Surface composition of the TiO<sub>2</sub> and B-TiO<sub>2</sub> catalysts was analyzed by XPS. **Fig.2A**  
30 shows, as an example, the high-resolution XPS spectra of the B 1s spectral region  
31 corresponding to 12B-TiO<sub>2</sub> catalyst. The binding energy for B 1s core level in H<sub>3</sub>BO<sub>3</sub> or  
32 B<sub>2</sub>O<sub>3</sub> is centered at 193.0 eV (B-O bond), whereas B located in the TiO<sub>2</sub> lattice  
33 corresponding to B occupying O sites as B-Ti bond in TiB<sub>2</sub> or O-Ti-B, and interstitial B  
34 as Ti-O-B presents lower binding energies at 187.5, 189.6 and 191.7 eV, respectively  
35 [16,18,19]. The symmetric peak found for all the B-TiO<sub>2</sub> catalysts was at 192.6 eV, thus  
36 indicating that B is mainly as H<sub>3</sub>BO<sub>3</sub> or B<sub>2</sub>O<sub>3</sub> in the catalysts surface, according to XRD  
37 results. However, the shift observed from 193.0 eV may be also indicative of the  
38 contribution of interstitial B. The presence of substitutional B (O-Ti-B or TiB<sub>2</sub>) can be  
39 disregarded according to the absence of signal at binding energies lower than 190 eV.  
40 Ti 2p spectral region for 12B-TiO<sub>2</sub> and TiO<sub>2</sub> catalysts is depicted in **Fig.2B**. The binding

1 energy of the Ti 2p core levels at 464.5 and 458.7 eV, and the separation of the peaks  
2 around 5.8 eV, confirm the valence state of Ti(IV) in TiO<sub>2</sub> [20,21]. However, for 12B-  
3 TiO<sub>2</sub> catalysts the peaks have been shifted towards higher binding energy values that  
4 can be explained on the basis of the higher electronegativity of boron, thus confirming  
5 the formation of Ti-O-B structures (interstitial B) [16]. Finally, **Fig.2C** shows the high-  
6 resolution XPS spectra of O 1s spectral region for TiO<sub>2</sub> and 12B-TiO<sub>2</sub> catalysts. The  
7 main peak located around 530 eV corresponds to Ti-O bonds with a widening at higher  
8 binding energy that has been assigned to hydroxyl groups in the TiO<sub>2</sub> surface. On the  
9 other hand, a second contribution to the O 1s spectra is observed in the boron doped  
10 catalyst at 532.4 eV corresponding to B-O bonds in H<sub>3</sub>BO<sub>3</sub> or B<sub>2</sub>O<sub>3</sub> [18]. Boron to  
11 titanium atomic surface ratio was calculated for all the catalysts from peak areas and  
12 Wagner atomic sensitivity factors [22]. These results are summarized in **Table 1**  
13 together with B/Ti bulk ratio calculated from ICP results. It can be noticed that the  
14 surface ratios are larger than bulk ratios, suggesting that most of B is located on the  
15 surface of TiO<sub>2</sub> during the sol-gel synthesis. This has also been previously reported in  
16 La-B co-doped TiO<sub>2</sub> catalysts [14,23].

17 **Table 1** also reports the band gap energy of the catalysts determined according to  
18 Tauc's expression from the UV-Vis diffuse reflectance spectra (**Fig.S3** and **Fig.S4** of  
19 the supplementary material). The E<sub>g</sub> value for bare TiO<sub>2</sub> was 3.07 eV, whereas for B-  
20 doped catalysts fluctuated from 3.01 to 3.12 eV with no distinguishable trend with the  
21 increasing B content. This is in a good agreement with previous results from Zaleska et  
22 al. [18] who reported similar values of E<sub>g</sub> for B-doped TiO<sub>2</sub> catalysts with B content from  
23 0.5 to 10 wt.%. This is likely the result of low or no mixing of 2p boron bands with 2p  
24 oxygen bands since no substitutional B is achieved [5].

25 The catalysts were tested in photocatalysis and photocatalytic ozonation of the  
26 selected pesticides DIU, MCPA, TBA and OPP (not shown). However, during the  
27 experiments, dissolved boron was detected in the reaction medium, suggesting  
28 leaching to some extent. To analyze the leaching phenomenon, the catalysts were  
29 submitted to water washing at the same conditions of the reaction medium (catalyst  
30 concentration and pH). These results for 12B-TiO<sub>2</sub> photocatalyst are depicted in **Fig.3**  
31 together with the evolution of dissolved boron during the photocatalytic ozonation  
32 treatment. It can be noticed that unstable boron was leached from the catalyst surface  
33 to the aqueous solution just at the beginning of the test and then remained constant up  
34 to 2 h. The differences found between pesticides solution or water washing are lower  
35 than 1 mgL<sup>-1</sup> of B and can be due to experimental deviations.

36 Total boron leached from all the catalysts during the washing procedure is summarized  
37 in **Table 2**. Boron concentration in solution reached values as high as 5.5 mgL<sup>-1</sup> in the  
38 case of the highest loading B-doped catalyst, being the loss of the total boron from 46  
39 to 70%. To our knowledge, boron leaching phenomenon has not been previously  
40 considered in B-doped TiO<sub>2</sub> catalysts application to wastewater treatment but it is  
41 mandatory since the limit of B ions in drinking water is 1 mg L<sup>-1</sup> according to the  
42 European Union standards [24].

1 On the basis of these results, two of the catalysts were washed with ultrapure water  
2 until no dissolved boron was detected (6B-TiO<sub>2</sub>-w and 12B-TiO<sub>2</sub>-w catalysts). Some  
3 characterization results of the washed samples are summarized in **Table 1**. It can be  
4 observed a decrease of B bulk content until 0.42-0.49%. The similar percentage of  
5 boron after washing both catalysts suggests that only this amount can be introduced in  
6 the TiO<sub>2</sub> lattice regardless of the initial amount of boron used. XRD patterns of the  
7 washed catalysts do not display the diffraction peak of boron species H<sub>3</sub>BO<sub>3</sub> or B<sub>2</sub>O<sub>3</sub>  
8 but, as expected, the washing procedure did not substantially modify the crystal size of  
9 the anatase phase. In this line, it is reasonable to assume that no significant changes in  
10 the textural properties due to washing procedure develop. On the other hand, the  
11 washed catalysts were analyzed by XPS and the results of 12B-TiO<sub>2</sub>-w are also plotted  
12 in **Fig.2** for comparative purposes. First of all, the intensity of the B 1s core level signal  
13 decreased significantly as a result of the loss of boron. However, the peak position  
14 located at 191.7 eV confirms the existence of boron in interstitial positions in the TiO<sub>2</sub>  
15 lattice (Ti-O-B bonds). The Ti 2p and O 1s spectra of 12B-TiO<sub>2</sub>-w catalyst were similar  
16 to those of bare TiO<sub>2</sub>. These results seem to point out that only a small portion of the  
17 initial boron was introduced as interstitial boron in the TiO<sub>2</sub> lattice during the sol-gel  
18 method used, and also that this B is strongly bonded and stable in aqueous suspension  
19 whereas the surface boron forming H<sub>3</sub>BO<sub>3</sub> or B<sub>2</sub>O<sub>3</sub> entities is easily dissolved. Two  
20 extra catalysts were prepared increasing the calcination time from 30 min to 1 h and 3  
21 h, but this operating variable did not improve the B stability leading to similar results  
22 (not shown). In addition, besides the band gap, other optical properties of the catalysts  
23 such absorption and scattering could be modified through B incorporation. The  
24 transmitted photon flux through a catalyst suspension could be an indirect  
25 measurement of these properties. In that case, the percentage of transmitted photon  
26 flux was 58.1% for TiO<sub>2</sub>, 47.7% for 6B-TiO<sub>2</sub>-w and 76.7% for 12B-TiO<sub>2</sub>-w. According to  
27 this, 6B-TiO<sub>2</sub>-w is expected to make a better use of radiation although no trend with  
28 other properties was observed and additional analyses would be necessary to reach  
29 stronger conclusions.

### 30 **3.2. Photocatalytic activity**

31 B-doped washed catalysts were tested in the photocatalytic oxidation and  
32 photocatalytic ozonation of the selected pesticides and compared with bare TiO<sub>2</sub> using  
33 simulated solar light as radiation source. The evolution of DIU, MCPA, TBA and OPP  
34 during photocatalytic oxidation treatment is depicted in **Fig.4**. The catalysts were stirred  
35 with the solution of the pesticides in the dark for 30 min to reach the adsorption  
36 equilibrium. Low adsorption capacity was observed for DIU, MCPA and OPP whereas  
37 around 20% of TBA adsorption was achieved. In general, the adsorption capacity  
38 increased in the B-doped catalysts likely due to their more developed surface area and  
39 porosity. Direct photolysis of the pesticides did not produce significant degradation of  
40 DIU, MCPA and TBA, though a slight decrease of OPP concentration up to 10% was  
41 observed. These results are consistent with the UV-Vis absorbance spectra of the  
42 target compounds shown in **Fig.S5**. For photocatalytic oxidation with bare and B-doped  
43 TiO<sub>2</sub> photocatalysts, in general, the presence of the catalyst improves the depletion



1 rate of all the pesticides, which show different reactivity in the mixture. The order of the  
2 reactivity was found to be MCPA>OPP>DIU>TBA. The rate constants of the reaction  
3 between these compounds and the hydroxyl radical are  $k_{MCPA-HO}=4.5 \times 10^9$ ,  $k_{OPP-}$   
4  $HO=9.8 \times 10^9$ ,  $k_{DIU-HO}=7.1 \times 10^9$ ,  $k_{TBA-HO}=2.8 \times 10^9 \text{ M}^{-1}\text{s}^{-1}$  [25,26]. It is commonly assumed  
5 that in photocatalytic oxidation, the main degradation of organics takes place through  
6 hydroxyl radicals, especially when direct photolysis and/or adsorption have negligible  
7 contributions. The highest degradation rate of MCPA was not in agreement with the  
8 order of reactivity derived from the rate constant values. It could be possible that the  
9 hydroxyl radical reaction was not the only predominant degradation route for MCPA. In  
10 fact, some organic peroxyradicals formed as intermediates during MCPA photocatalytic  
11 oxidation are responsible of an autocatalytic behavior, as previously reported [27].

12 The incorporation of B to the catalysts lattice conferred an important effect in its  
13 catalytic activity. Thus, the degradation rate of all the pesticides was clearly enhanced  
14 in the presence of 6B-TiO<sub>2</sub>-w and 12B-TiO<sub>2</sub>-w catalysts. Similar behavior was observed  
15 for DIU and OPP, as 70-80% degradation was achieved with 12B-TiO<sub>2</sub>-w catalyst vs.  
16 20-30% obtained with bare TiO<sub>2</sub>. For MCPA, around 45 min were necessary to reach  
17 almost complete removal whereas around 10% of MCPA still remained in solution with  
18 TiO<sub>2</sub> after 120 min of treatment. TBA depletion also improved with B-doped catalysts,  
19 reaching around 50% degradation compared to 35% with TiO<sub>2</sub>. However, TBA showed  
20 a refractory character towards its photocatalytic oxidation, since its concentration  
21 decreased faster during the first 15 min and then the degradation rate slowed down.  
22 These results point out the benefits of incorporating boron to the TiO<sub>2</sub> lattice. The role  
23 of B in interstitial positions of TiO<sub>2</sub> has not been unequivocally defined. It seems that B  
24 tends to lose its three valence electrons, which are donated to the 3d states of lattice Ti  
25 ions, thus giving rise to Ti(III) species. These latter have been postulated to reduce the  
26 recombination of photoexcited electrons and holes [5,28]. A boron content of about 0.5  
27 wt.% seems to be enough to enhance the photocatalytic activity of TiO<sub>2</sub>. The  
28 differences found in the activity of both doped catalysts could be related to the higher  
29 content of surface B detected by XPS in the 12B-TiO<sub>2</sub>-w catalyst. On the other hand,  
30 the differences found in the textural properties and crystallinity of bare TiO<sub>2</sub> and B-TiO<sub>2</sub>  
31 catalysts might also play an important role in the behavior of the catalysts. However, it  
32 has been reported the improvement of photocatalytic performance with the increased  
33 crystallinity of the anatase particles since recombination process is prevented to some  
34 extent, though larger crystal size leads to lower specific surface areas [29]. Therefore,  
35 the improvement observed in the catalytic activity could be related to the presence of  
36 boron in TiO<sub>2</sub> interstitial positions more than to the changes produced in TiO<sub>2</sub> crystal  
37 size and textural properties. Also, the modification on the radiation absorption and  
38 scattering properties cannot be disregarded although transmitted photon flux  
39 measurements were not conclusive at this respect.

40 The evolution of the pesticides concentration during photocatalytic ozonation is shown  
41 in **Fig.5**. Also, for comparative purposes, ozonation alone and the combination of  
42 ozone and radiation (photolytic ozonation) were applied. It can be observed that,  
43 regardless of the presence of catalysts and/or radiation, all the ozone treatments led to

1 higher degradation rate of the pesticides than the photocatalytic oxidation process. The  
2 average time needed to reach 99% of pesticides removal with ozone treatments was  
3 around 60 min for DIU and TBA, and 30 min for MCPA and OPP. These are, in  
4 general, in agreement with the values of the rate constants of the ozone-pesticide  
5 reaction ( $k_{MCPA-O_3}=323$ ,  $k_{OPP-O_3}=379$ ,  $k_{DIU-O_3}=3.7$ ,  $k_{TBA-O_3}=20 \text{ M}^{-1}\text{s}^{-1}$  [25,30,31]).  
6 Nevertheless, indirect reactions due to ozone decomposition into hydroxyl radicals  
7 could take place at the reaction pH [32,33], also according with the high rate constant  
8 values between hydroxyl radical-pesticides commented above.

9 Main differences among the ozone treatments were found in terms of TOC removal.  
10 Previously, as seen in **Fig.6**, in all cases, after the dark stage, low TOC removal due to  
11 adsorption on the catalysts was observed in comparison of the reaction stage.  
12 However, doped catalysts presented higher adsorption capacity compared to bare  
13  $\text{TiO}_2$ , probably due to their higher surface areas. On the other hand, the TOC removal  
14 observed in the direct photolysis run was negligible, as expected. These results were  
15 improved by photocatalytic oxidation reaching 25% TOC removal with bare  $\text{TiO}_2$  after 2  
16 h. This mineralization level increased up to 37% and 45% using 6B- $\text{TiO}_2$ -w and 12B-  
17  $\text{TiO}_2$ -w catalysts, respectively. The higher efficiency of the doped catalysts compared to  
18 that of bare  $\text{TiO}_2$  was also observed when applying the combined photocatalytic  
19 ozonation treatment. Although only 20% of the contaminant mixture was mineralized by  
20 single ozonation, the presence of radiation during photolytic ozonation increased up to  
21 45% the mineralization degree. In the presence of radiation, a fraction of the ozone  
22 molecules that have not directly reacted with contaminants are photolyzed under  
23 wavelengths near to 300 nm to produce reactive oxygen species (ROS), which  
24 enhance the mineralization rate [34]. These results were highly improved with the  
25 photocatalytic ozonation treatment, reaching 65-70% TOC removal. Ozone, as an  
26 electrophilic molecule, can trap electrons from the conduction band of the catalyst  
27 yielding ozonide ion radicals that decompose into ROS [7,8]. B-doped catalysts were  
28 more active than bare  $\text{TiO}_2$  and led to faster mineralization rate according to TOC  
29 removal reached at 60 min reaction time, though the final mineralization degree was  
30 similar (around  $1 \text{ mg L}^{-1}$  TOC is the difference between bare and doped- $\text{TiO}_2$  catalysts  
31 at the end of the treatment).

32 It is known that hydrogen peroxide can be generated during photocatalytic treatments  
33 and also through direct ozone reactions [35,36,37]. The role of  $\text{H}_2\text{O}_2$  and  $\text{O}_3$  involved in  
34 photocatalytic reactions has been analyzed through the results depicted in **Fig.7**. When  
35 comparing the dissolved ozone profiles (**Fig.7A**) for single ozonation and photolytic  
36 ozonation it is observed that ozone accumulated in the solution from the beginning and  
37 its concentration remained almost constant along the experiment in contrast to  
38 photolytic ozonation which presented a maximum in the ozone concentration, which  
39 then decreased dramatically. This suggests that ozone is photolyzed with the radiation  
40 used to give rise to ROS, which enhanced the mineralization rate. The low  
41 accumulation of ozone in solution during the photocatalytic ozonation experiment can  
42 be explained taking into account the electrophilic character of ozone, which can act as  
43 an electron acceptor and trap the electrons photogenerated on the photocatalysts

1 surface. On the other hand, the hydrogen peroxide concentration evolution is also  
2 shown in **Fig.7B**. Photolysis and photocatalytic oxidation gave place to very low H<sub>2</sub>O<sub>2</sub>  
3 concentrations. However, in all the ozone treatments the concentration of hydrogen  
4 peroxide was significantly higher. Thus, the formation of H<sub>2</sub>O<sub>2</sub> through direct ozone  
5 reactions of the four pesticides was experimentally confirmed. During single ozonation,  
6 H<sub>2</sub>O<sub>2</sub> concentration increased up to 40 min and then remained almost constant until the  
7 end of the experiment. A higher H<sub>2</sub>O<sub>2</sub> decomposition rate was observed during  
8 photolytic ozonation, resulting in lower concentration at the end of the treatment. The  
9 H<sub>2</sub>O<sub>2</sub> could undergo photolytic decomposition under wavelengths near 300 nm, thus  
10 improving the degradation and mineralization of the contaminants [38]. On the other  
11 hand, during photocatalytic ozonation with bare TiO<sub>2</sub> a higher decomposition rate of  
12 H<sub>2</sub>O<sub>2</sub> was also observed, the concentration being negligible after 100 min of treatment.  
13 With B-doped TiO<sub>2</sub> catalysts, the formation of hydrogen peroxide took place at higher  
14 rate reaching a maximum concentration at about 20 min and then the consumption was  
15 also faster and the concentration negligible at the end of the treatment. These results  
16 point out that H<sub>2</sub>O<sub>2</sub> is likely being consumed through photocatalytic reactions acting as  
17 electron acceptor in the TiO<sub>2</sub> surface. This process is more efficient with B-doped TiO<sub>2</sub>  
18 catalysts compared to bare TiO<sub>2</sub> also indicating their higher photocatalytic activity.

### 19 **3.3. Catalyst stability**

20 The stability and reusability of the 12B-TiO<sub>2</sub>-w catalyst was tested in three consecutive  
21 runs of photocatalytic ozonation process. The catalyst was easily separated by  
22 sedimentation after each run and used without any treatment in the next experiment.  
23 After removing the supernatant solution, a new fresh solution of the four pesticides was  
24 added to start the following run. In all the experiments the catalyst from the previous  
25 run was kept 30 min in the darkness with the new fresh solution to reach adsorption  
26 equilibrium.

27 Taking into account that main differences found between the ozone treatments were  
28 found in mineralization, **Fig.8** shows TOC removal percentages during the dark  
29 adsorption stage and after 1 and 2 hours of photocatalytic ozonation. During the dark  
30 stage, only slight changes were observed in adsorption capacity of the reused catalyst  
31 varying the percentage of TOC adsorbed between 3-7% with no trend which indicates  
32 that the small amount of initial pesticides adsorbed onto the catalyst surface is oxidized  
33 during the photocatalytic treatment. On the other hand, the mineralization reached at 2  
34 h reaction time was maintained at about 75% during the consecutive runs.  
35 Furthermore, the mineralization rate seems to slightly increase when compared TOC  
36 removal at 1 h reaction time being mineralization increased from 55 to 65% during the  
37 reutilization of the catalyst. In addition no boron leached was detected after the  
38 consecutive use of the catalyst. Therefore, although additional experiments would be  
39 needed to test the long term performance of the catalyst, this results point out the  
40 stability and reusability of these B-doped TiO<sub>2</sub> catalysts once the non-structural  
41 remaining boron was washed.

### 42 **4. Conclusions**

1 The sol-gel method used to dope the TiO<sub>2</sub> catalysts led to the incorporation of a lower  
2 amount of boron than the theoretical value. A part of the amount of boron on the  
3 catalysts was in the form of B<sub>2</sub>O<sub>3</sub>/H<sub>3</sub>BO<sub>3</sub> species, which was unstable in aqueous  
4 solution and released boron to the reaction medium. An extra washing of the catalysts  
5 with water led to the removal of unstable boron and no further leaching. The rest of the  
6 boron on the catalysts was incorporated in interstitial positions of TiO<sub>2</sub> and did not  
7 modify the band gap energy with respect to bare TiO<sub>2</sub>. The presence of boron on the  
8 catalysts also caused the reduction of the crystal size of the anatase particles of TiO<sub>2</sub>  
9 and an increase of the pore volume and specific surface area respect to the bare TiO<sub>2</sub>.  
10 The washed B-doped TiO<sub>2</sub> were more active than bare TiO<sub>2</sub> for the removal and  
11 mineralization of the target compounds due to the effect of boron in interstitial positions  
12 of TiO<sub>2</sub> avoiding the recombination process to some extent. The efficiency of the  
13 studied systems regarding mineralization rate followed the order: single ozonation <  
14 photocatalysis with TiO<sub>2</sub> < photocatalysis with B-TiO<sub>2</sub> < photolytic ozonation <  
15 photocatalytic ozonation with TiO<sub>2</sub> < photocatalytic ozonation with B-TiO<sub>2</sub>.  
16 Photocatalytic ozonation with B-TiO<sub>2</sub> catalysts was the most efficient process in terms  
17 of mineralization and ozone consumption, leading to the complete removal of the  
18 pesticides in less than 90 min with 75% mineralization after 120 min. The catalytic  
19 activity was maintained after 3 consecutive runs with no leaching boron detected.

## 20 **Appendix A. Supplementary data**

21 Supplementary data associated with this article can be found, in the online version, at  
22 XXXXXX

## 23 **Acknowledgements**

24 This work has been supported by the Spanish Ministerio de Economía y  
25 Competitividad (MINECO) and European Feder Funds through the project CTQ2012-  
26 35789-C02-01. Authors acknowledge the SAIUEX service of the University of  
27 Extremadura for the characterization analyses. D. H. Quiñones thanks the MINECO the  
28 concession of a predoctoral FPI grant and an aid for a research stay at the  
29 Loughborough University.

## 30 **References**

- 
- [1] A. Calzadilla, K. Rehdanz, R. Tol. *J. Hydrology*, 384 (2010) 292-305.
- [2] A. Fujishima, T. N. Rao, D. A. Tryk. *J. Photochem. Photobiol. C Photochem. Rev.* 1 (2000) 1-21.
- [3] X. Gao , P. Chen , J. Liu. *Mater. Let.* 65 (2011) 685–687.
- [4] P. Dharmarajan, A. Sabastiyam, M. Yosuva Suvaikin, S. Titus, C. Muthukumar. *Chemical Science Transactions*, 2 (2013) 1450-1458.
- [5] M.V. Dozzi, E. Selli. *J. Photochem. Photobiol. C: Photochem. Rev.* 14 (2013) 13-28.
- [6] N. S. Begum, H. M. F. Ahmed, O. M. Hussain. *Bull. Mater. Sci.* 31 (2008) 741–745.

- 
- [7] E. M. Rodríguez, G. Márquez, E. A. León, P. M. Álvarez, A. M. Amat, F. J. Beltrán. *J. Environ. Manag.* 127 (2013) 114-124.
- [8] T.E. Agustina, H.M. Ang, V.K. Vareek, *J. Photochem. Photobiol. C Photochem. Rev.* 6 (2005) 264-273.
- [9] Z. Li, B. Gao, G. Z. Chen, R. Mokaya, S. Sotiropoulos, G. Li Puma. *Appl. Catal. B Environ.* 110 (2011) 50-57.
- [10] V. Loddo, M. Addamo, V. Augugliaro, L. Palmisano, M. Schiavello, E. Garrone. *AIChE J.* 52 (2006) 2565-2574.
- [11] H. Bader, J. Hoigné. *Water Res.* 15 (1981) 449-456.
- [12] W. Masschelein, M. Denis, R. Ledent. Spectrophotometric determination of residual hydrogen peroxide. *Water Management. Water Sewage Works*, August (1977) 69-72.
- [13] F.J. López, E. Giménez, F. Hernández. *Fresenius J. Anal. Chem.* 346 (1993) 984.
- [14] J.W. Liu, R. Han, H.T. Wang, Y. Zhao, W.J. Lu, H.Y. Wu, T.F. Yu, Y.X. Zhang. *J. Mol. Catal. A Chem.* 344 (2011) 145-152.
- [15] S. Bagwasi, B. Tian, J. Zhang, M. Nasir. *Chem. Eng. J.* 217 (2013) 108-118.
- [16] W. Zhang, T. Hu, B. Yang, P. Sun, H. He. *J. Adv. Oxid. Technol.* 16 (2013) 261-267.
- [17] D. Chen, D. Yang, Q. Wang, Z. Jiang, *Ind. Eng. Chem. Res.* 45 (2006) 4110-4116.
- [18] A. Zaleska, J.W. Sobczak, E. Grabowska, J. Hupka. *Appl. Catal. B Environ.* 78 (2008) 92-100.
- [19] E. Finazzi, C. Di Valentin, G. Pacchioni. *J. Phys. Chem. C* 113 (2009) 220-228.
- [20] M.W. Xiao, L. Wang, X.J. Huang, Y.D. Wu, Z. Dang. *J. Alloys Comp.* 470 (2009) 486-491.
- [21] Y. Li, L. Chen, Y. Guo, X. Sun, Y. Wei. *Chem. Eng. J.* 181-182 (2012) 734-739
- [22] C.D. Wagner, L.E. Davis, M.V. Zeller, J.A. Taylor, R.H. Raymond, L.H. Gale. *Surf. Interf. Anal.* 3 (1981) 211-225
- [23] X. Lan, L. Wang, B. Zhang, B. Tian, J. Zhang. *Catal. Today* 224 (2014) 163-170.
- [24] Council of the European Union, Council Directive 98/83/EC of 3 November 1998. On the quality of water intended for human consumption (1998).
- [25] M. Olak-Kucharczyk, J.S. Miller, S. Ledakowicz. Ozonation kinetics of o-phenylphenol in aqueous solutions. *Ozone. Sci. Eng.* 34 (2012) 300-305.

- 
- [26] B.A. Wols, C.H.M. Hofman-Caris. *Water Res.* 46 (2012) 2815-2827.
- [27] J. Rivas, R.R. Solis, O. Gimeno, J. Sagasti. *Int. J. Environ. Sci. Technol.* December 2013, DOI 10.1007/s13762-013-0452-4.
- [28] V. Gombac, L. De Rogatis, A. Gasparotto, G. Vicario, T. Montini, D. Barreca, G. Calducci, P. Fornasiero, E. Tondello, M. Graziani. *Chem. Phys.* 339 (2007) 111.
- [29] M.A. Henderson. *Surf. Sci. Reports* 66 (2011) 185-297.
- [30] J.Y. Hu, T. Morita, Y. Magara, T. Aizawa. *Water Res.* 34 (2000) 2215-2222
- [31] F. J. Benítez, F. J. Real, J. L. Acero, C. García. *Water Res.* 41 (2007) 4073 – 4084.
- [32] U. von Gunten. *Water Res.* 37 (2003) 1443-1467.
- [33] F. J. Beltran. *Ozone reaction kinetics for water and wastewater systems.* Boca Raton, CRC Press, 2004, Florida (USA).
- [34] L. Sánchez, X. Domenech, J. Casado, J. Peral. *Chemosphere* 50 (2003) 1085-1093.
- [35] M. Mvula, C. von Sonntag. *Org. Biomol. Chem.* 1 (2003) 1749-1756.
- [36] A. Leitzke, C. von Sonntag. *Ozone Sci. Eng.* 31 (2009) 301-308.
- [37] S. Rakowski, D. Cherneva. *Int. J. Chem. Kinetics* 22 (1990) 321-329.
- [38] J.H. Baxendale, J.A. Wilson. *Trans. Faraday Soc.* 53 (1957) 344-356.

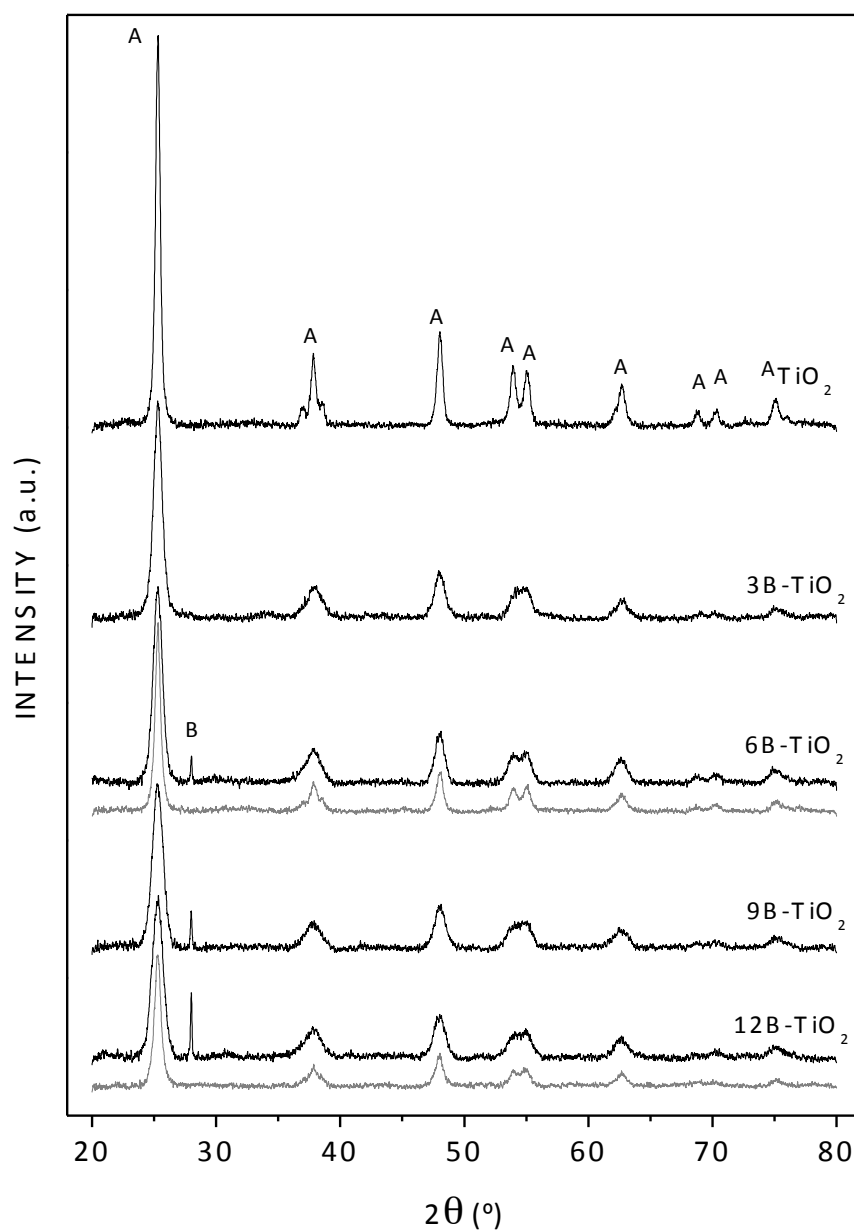


**Fig.1.** XRD patterns of the photocatalysts (Grey: washed samples, A: anatase, B: boron B<sub>2</sub>O<sub>3</sub>/H<sub>3</sub>BO<sub>3</sub>)

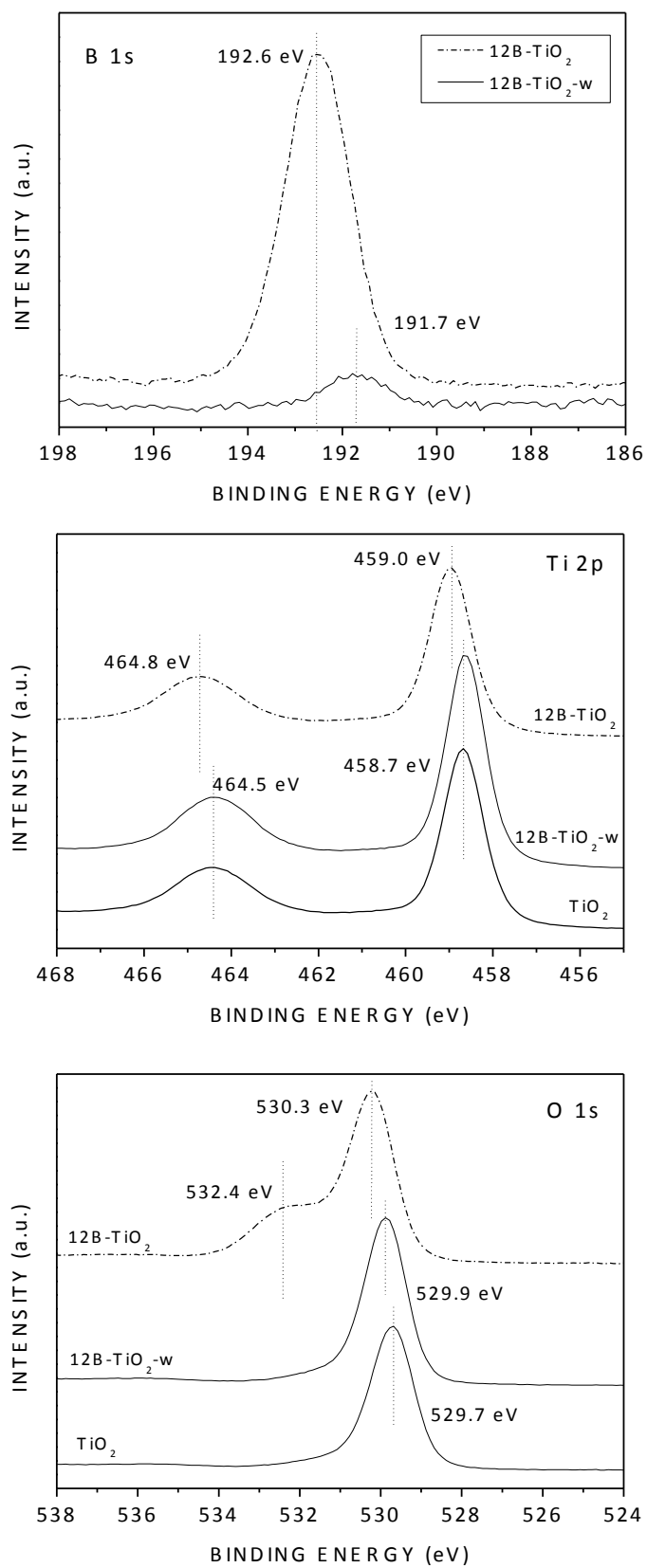


**Fig.2.** High resolution XPS spectra of B 1s, O 1s and Ti 2p spectral regions of the catalysts TiO<sub>2</sub>, 12B-TiO<sub>2</sub> and 12B-TiO<sub>2</sub>-w



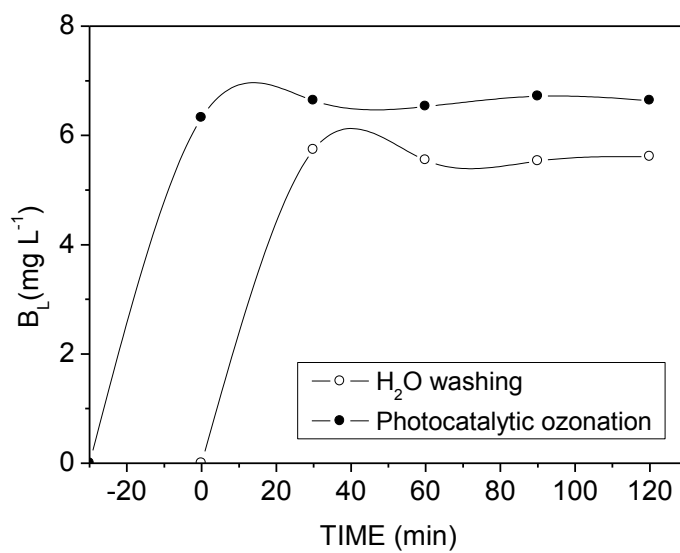


**Fig.3.** B leaching of the 12B-TiO<sub>2</sub> catalyst during washing procedure and photocatalytic ozonation reaction (0.33 g L<sup>-1</sup>)

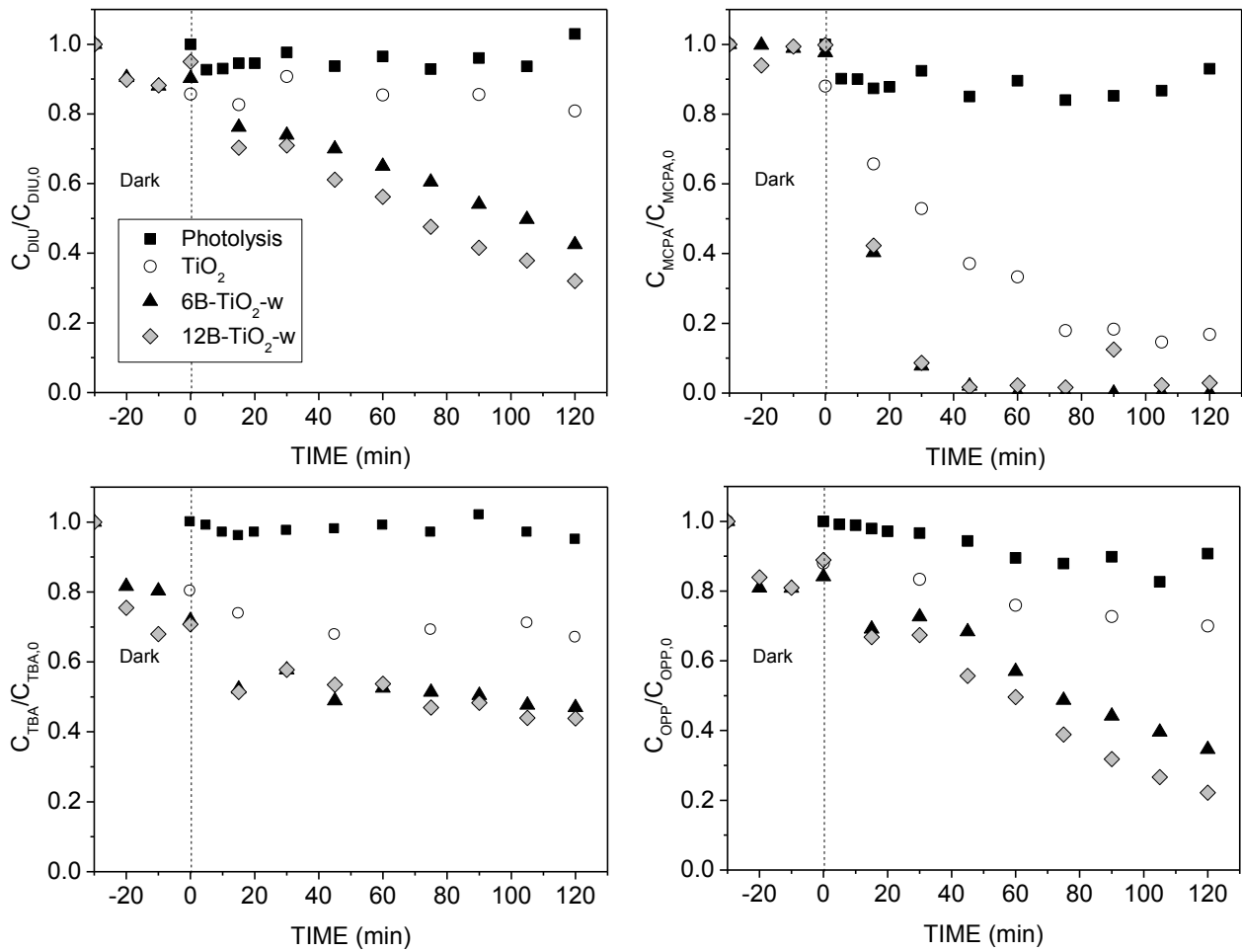


**Fig.4.** Evolution of dimensionless herbicides and pesticides concentration during photocatalysis with  $\text{TiO}_2$  and B- $\text{TiO}_2$  catalysts. Conditions:  $\text{pH}_0=6.5$ ,  $T=25\text{-}40^\circ\text{C}$ ,  $C_{\text{PES},0}=5 \text{ mg L}^{-1}$  (in the mixture),  $C_{\text{CAT}}=0.33 \text{ g L}^{-1}$ ,  $Q_g=10 \text{ L h}^{-1}$  ( $\text{O}_2$ ).

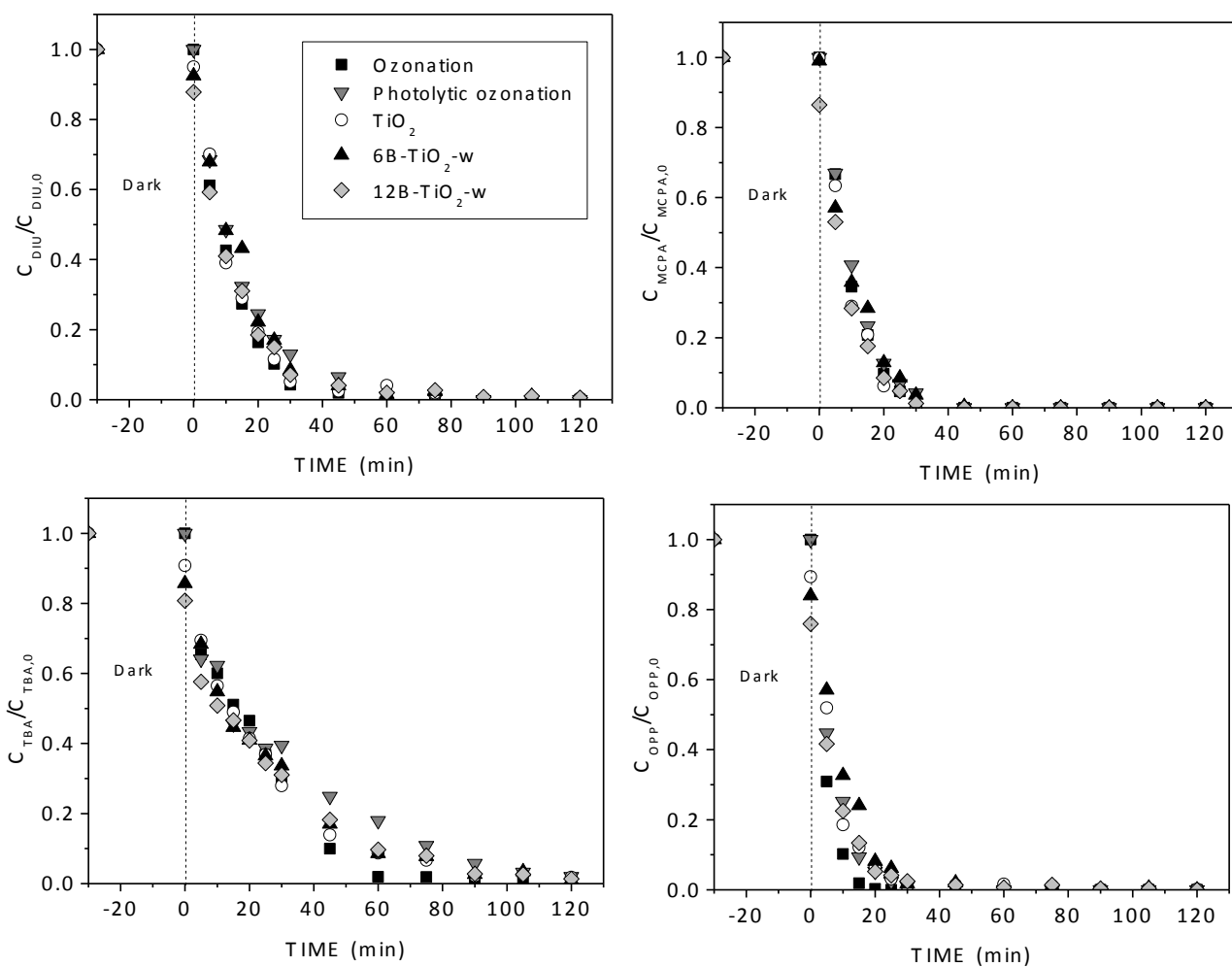


**Fig.5.** Evolution of dimensionless pesticides concentration during ozone treatments with TiO<sub>2</sub> and B-TiO<sub>2</sub> catalysts. Conditions: pH<sub>0</sub>=6.5, T=25-40°C, C<sub>PES,0</sub>=5 mg L<sup>-1</sup> (in the mixture), C<sub>CAT</sub>=0.33 g L<sup>-1</sup>, C<sub>O<sub>3</sub>inlet</sub>=5 mg L<sup>-1</sup>, Q<sub>g</sub>=10 L h<sup>-1</sup> (O<sub>3</sub>/O<sub>2</sub>).

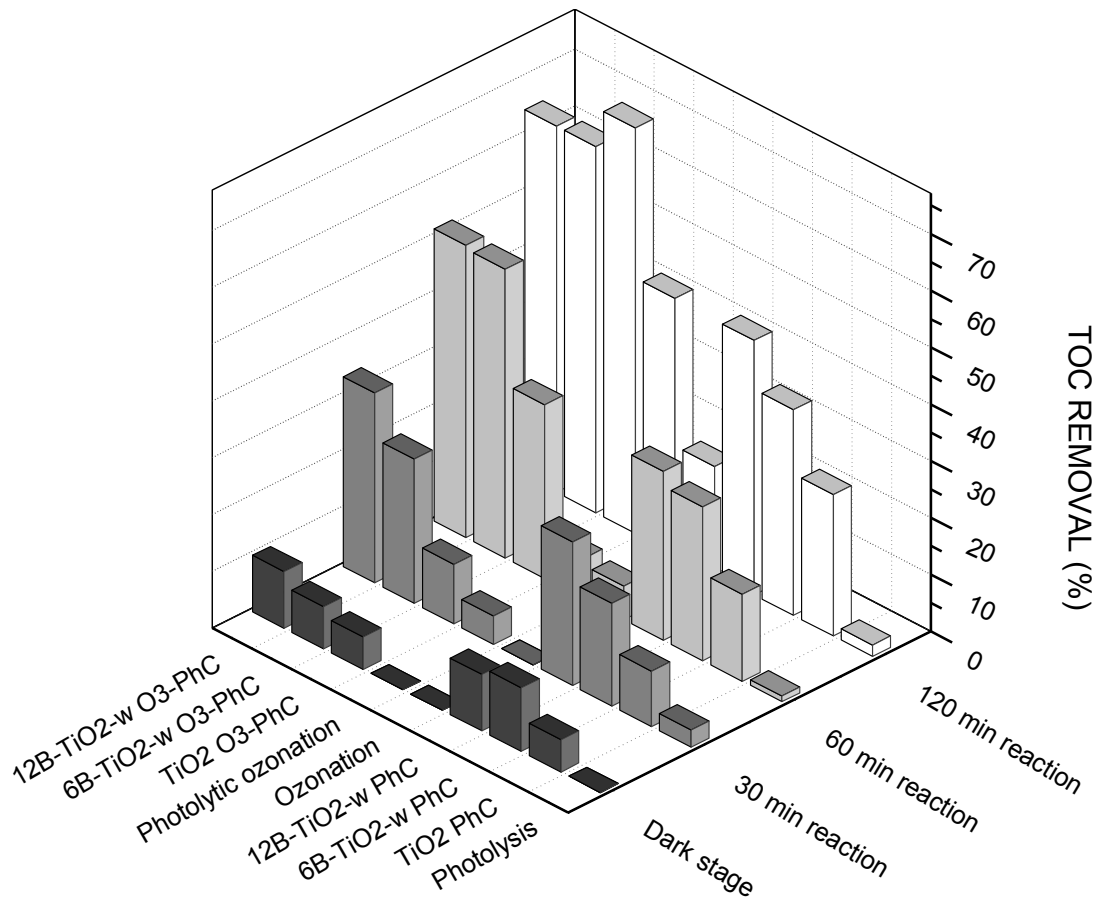


**Fig.6.** TOC removal during all the treatments applied with  $\text{TiO}_2$  and  $\text{B-TiO}_2$  catalysts. Conditions:  $\text{pH}_0=6.5$ ,  $T=25-40^\circ\text{C}$ ,  $C_{\text{PES},0}=5 \text{ mg L}^{-1}$  (in the mixture),  $C_{\text{CAT}}=0.33 \text{ g L}^{-1}$ ,  $C_{\text{O}_3\text{ginlet}}=5 \text{ mg L}^{-1}$ ,  $Q_g=10 \text{ L h}^{-1}$  ( $\text{O}_3/\text{O}_2$ ).

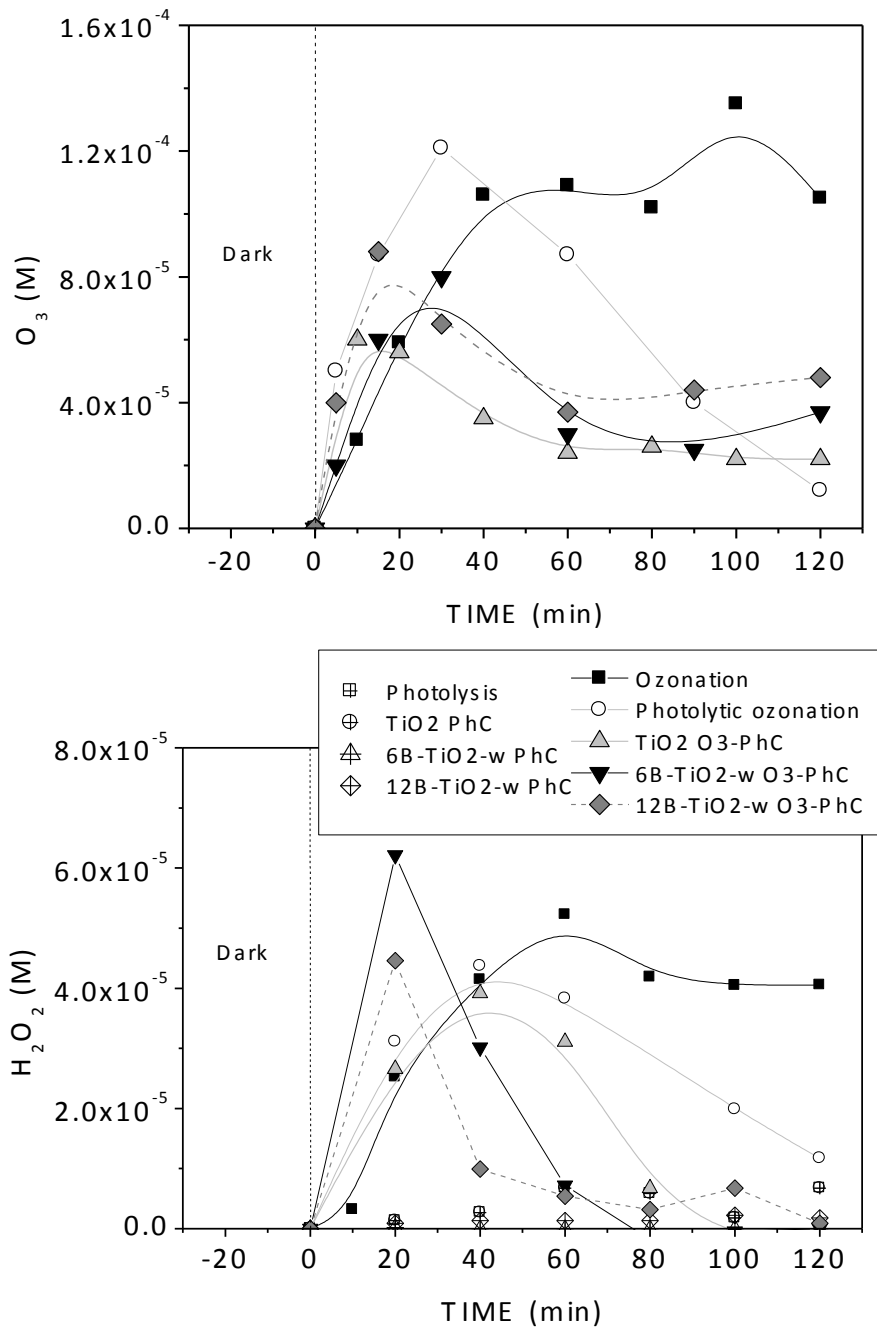


**Fig.7.** Evolution of dissolved  $O_2$  and  $H_2O_2$  concentrations during all the treatments applied. Conditions:  $pH_0=6.5$ ,  $T=25-40^\circ C$ ,  $C_{PES,0}=5 \text{ mg L}^{-1}$ ,  $C_{CAT}=0.33 \text{ g L}^{-1}$ ,  $C_{O_3\text{ginlet}}=5 \text{ mg L}^{-1}$  (in the mixture),  $Q_g=10 \text{ L h}^{-1}$  ( $O_3/O_2$ ).

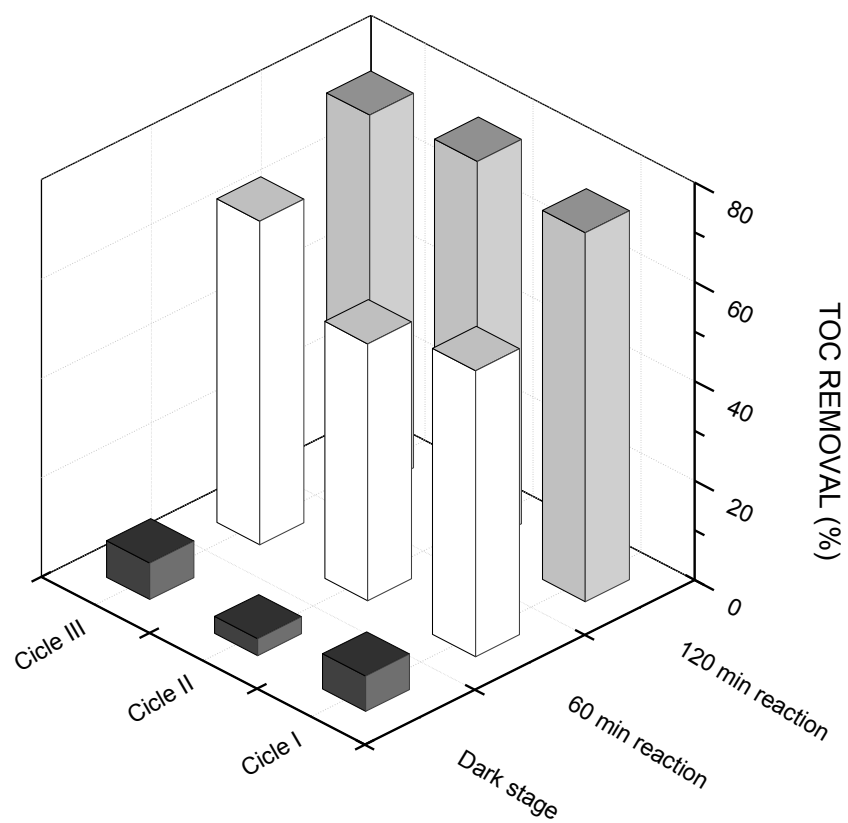


**Fig.8.** TOC removal during consecutive photocatalytic ozonation runs. Conditions:  $\text{pH}_0=6.5$ ,  $T=25\text{-}40^\circ\text{C}$ ,  $C_{\text{PES},0}=5 \text{ mg L}^{-1}$  (in the mixture),  $C_{\text{CAT}}=0.33 \text{ g L}^{-1}$ ,  $C_{\text{O}_3\text{ginlet}}=5 \text{ mg L}^{-1}$ ,  $Q_g=10 \text{ L h}^{-1}$  ( $\text{O}_3/\text{O}_2$ ).

**Table 1.** Nomenclature and some properties of the B-TiO<sub>2</sub> catalysts

CATALYST	B (wt.%)	d <sub>A</sub> (nm)	S <sub>BET</sub> (m <sup>2</sup> g <sup>-1</sup> )	V <sub>P</sub> (cm <sup>3</sup> g <sup>-1</sup> )	(B/Ti) <sub>ICP</sub> (at./at.)	(B/Ti) <sub>XPS</sub> (at./at.)	E <sub>g</sub> (eV)
TiO <sub>2</sub>	n.d.	16.8	68.3	0.102	0	0	3.07
3B-TiO <sub>2</sub>	0.91	9.9	121.3	0.209	0.068	0.469	3.12
6B-TiO <sub>2</sub>	1.06	9.2	120.1	0.147	0.079	0.531	3.03
9B-TiO <sub>2</sub>	1.81	7.6	122.4	0.163	0.137	0.541	3.05
12B-TiO <sub>2</sub>	3.55	7.5	125.5	0.180	0.273	0.693	3.01
6B-TiO <sub>2</sub> -w	0.42	9.8	n.m.	n.m.	0.031	0.018	n.m.
12B-TiO <sub>2</sub> -w	0.49	7.9	n.m.	n.m.	0.036	0.029	n.m.

n.d.: not detected, n.m.: not measured

**Table 2.** B leaching from the B-TiO<sub>2</sub> catalysts during washing procedure (0.33 g L<sup>-1</sup>)

CATALYST	B (mg L <sup>-1</sup> )	B (%)
TiO <sub>2</sub>	n.d.	n.d.
3B-TiO <sub>2</sub>	1.83	60.6
6B-TiO <sub>2</sub>	1.91	54.3
9B-TiO <sub>2</sub>	4.20	69.9
12B-TiO <sub>2</sub>	5.50	46.6

n.d.: not detected

## SUPPLEMENTARY INFORMATION

**Boron doped TiO<sub>2</sub> catalysts for photocatalytic ozonation of aqueous mixtures of common pesticides: Diuron, o-phenylphenol, MCPA and terbuthylazine**

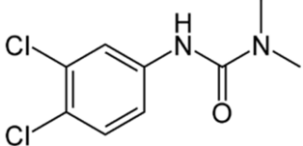
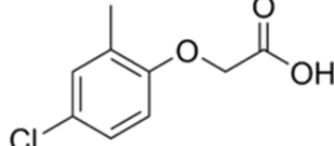
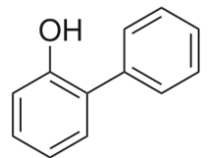
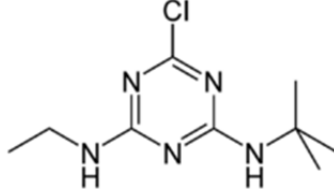
**D.H. Quiñones<sup>1</sup>, A. Rey<sup>1</sup>, P.M. Álvarez<sup>1</sup>, F.J. Beltrán<sup>1</sup>, G. Li Puma<sup>2</sup>**

<sup>1</sup>*Dpto. Ingeniería Química y Química Física, Universidad de Extremadura, Avda. Elvas s/n 06006 Badajoz (Spain)*

<sup>2</sup>*Environmental Nanocatalysis and Photoreaction Engineering, Department of Chemical Engineering, Loughborough University, LE11 3TU, Loughborough (United Kingdom)*

### Molecular structure of the selected pesticides

**Table S1.** Molecular structure of the selected pesticides

<b>DIURON (DIU)</b>	<b>2-METHYL-4-CHLOROPHENOXYACETIC ACID (MCPA)</b>
	
<b>ORTOPHENYLPHENOL (OPP)</b>	<b>TERBUTHYLAZINE (TBA)</b>
	



## Emission spectrum of the Suntest CPS solar simulator

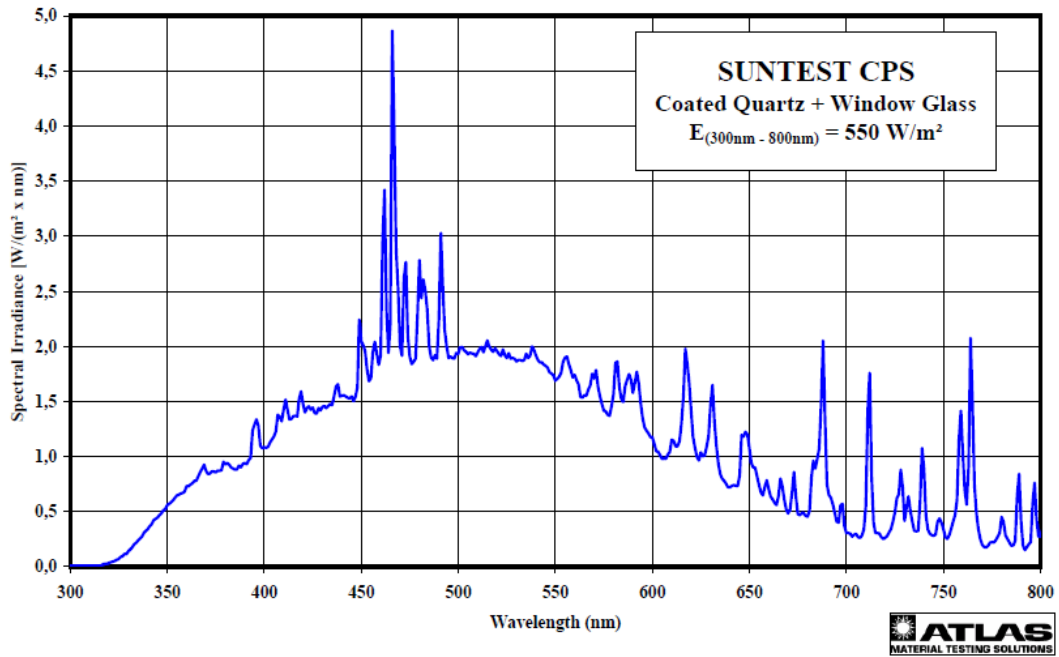
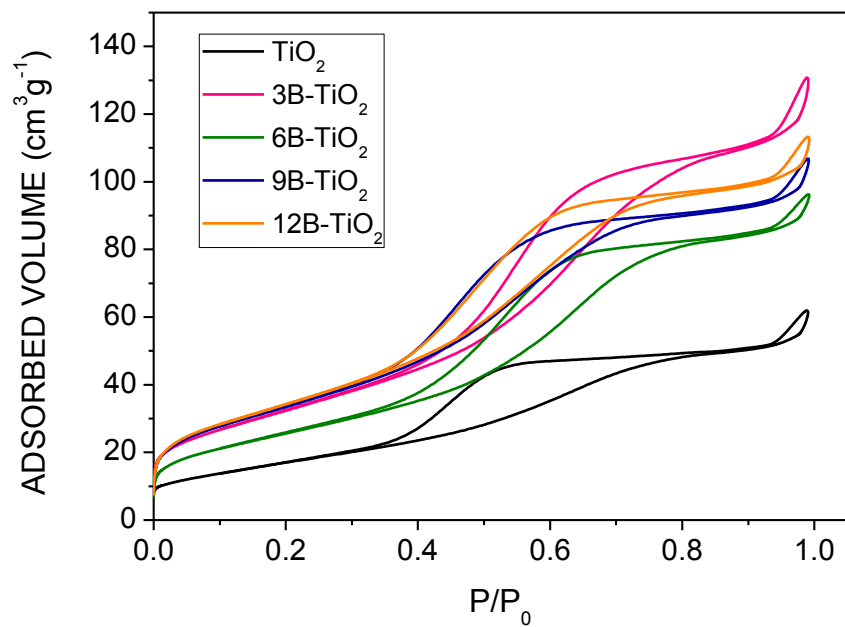


Fig.S1. Emission spectrum of the solar simulator

## Adsorption-desorption isotherm of the B-TiO<sub>2</sub> and CNT composite catalysts



**Fig.S2.** N<sub>2</sub> adsorption-desorption isotherms

### Absorbance spectra of TiO<sub>2</sub> and B-TiO<sub>2</sub> catalysts

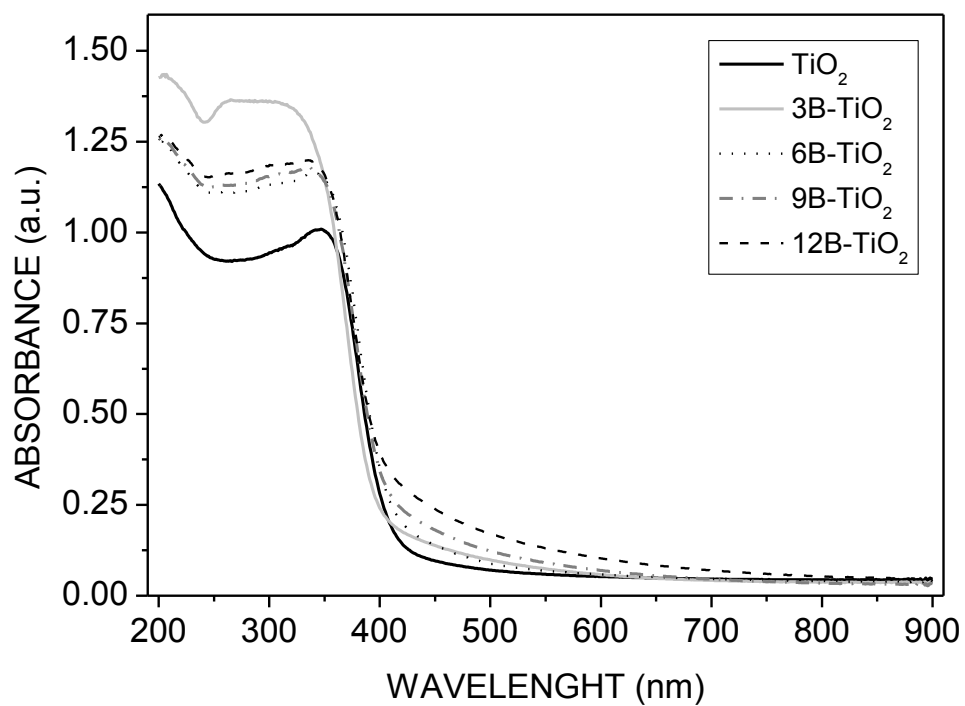


**Fig. S3.** DR-UV-Vis spectra of the catalysts

### Band-gap determination of TiO<sub>2</sub> and B-TiO<sub>2</sub> catalysts

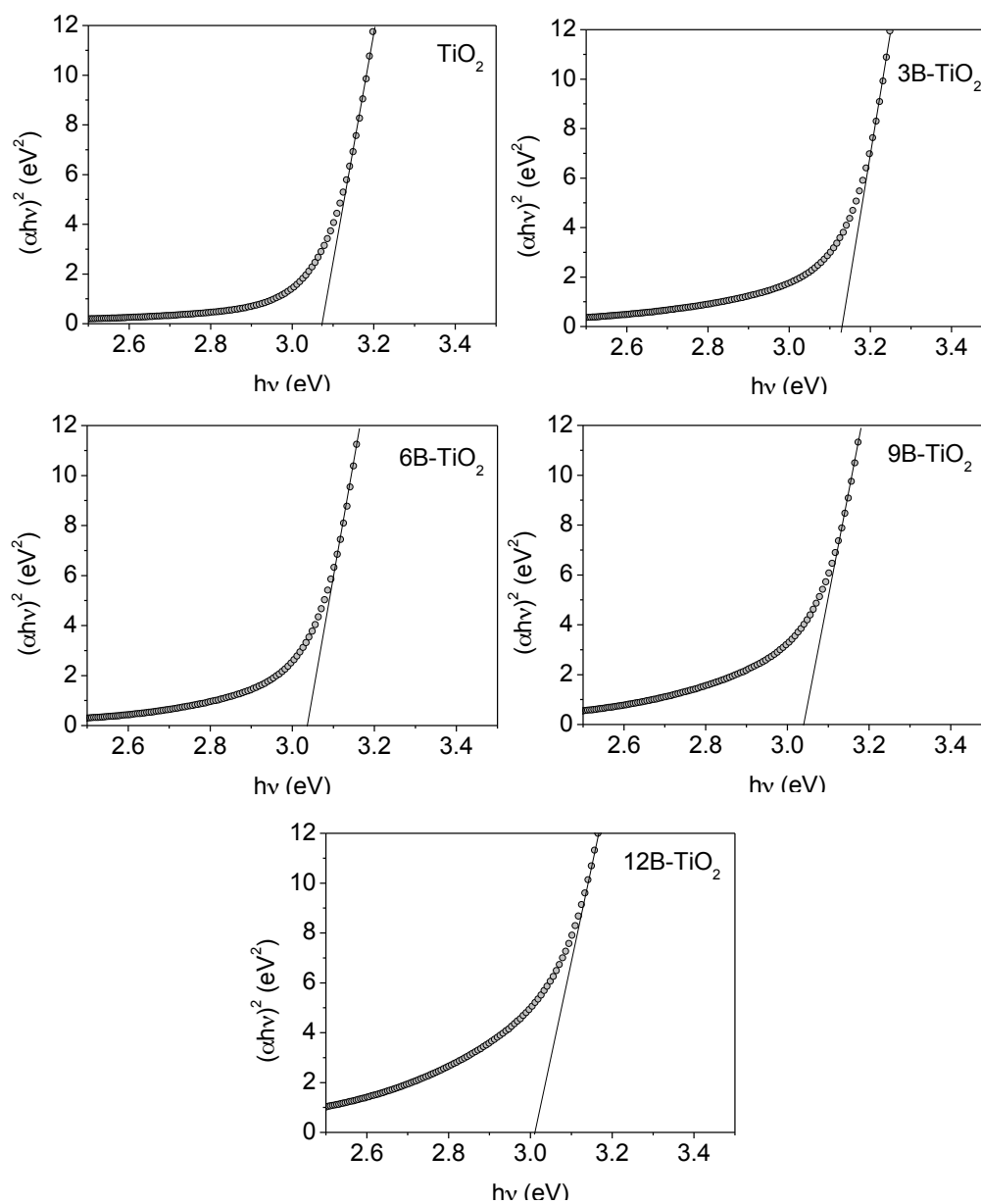


**Fig.S4.** Band-gap determination from DR-UV-Vis analysis of the B-doped catalysts

### UV-Vis Absorbance spectra of DIU, MCPA, OPP and TBA

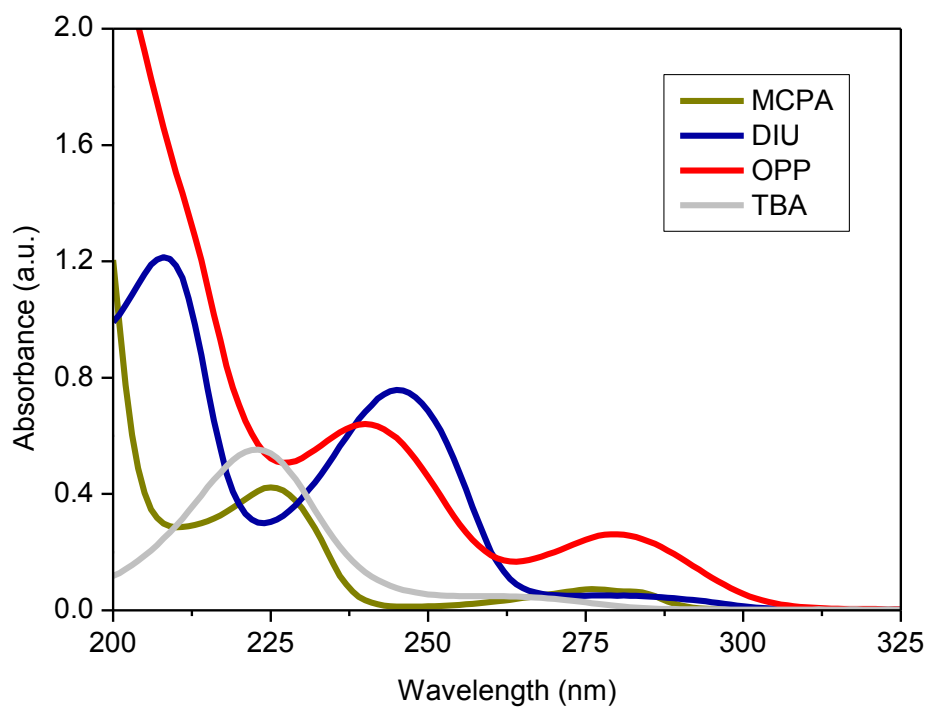


**Fig.S5.** Absorbance UV-Visible spectra of the target compounds in ultrapure water from 200-325 nm

## RESEARCH HIGHLIGHTS

- B-TiO<sub>2</sub> catalysts for photocatalytic ozonation of pesticides mixture.
- Leaching phenomena of non-structural boron.
- Beneficial effect of interstitial B in TiO<sub>2</sub> for photocatalytic ozonation.
- Stability and high efficiency of B-TiO<sub>2</sub> in mineralization and ozone consumption.
- Complete herbicide-pesticide removal with 75% mineralization after 2 h.

